IRF5 promotes influenza-induced inflammatory responses in human iPSC-derived myeloid cells and murine models

Running title: IRF5 promotes influenza-induced inflammatory responses

Jessica L Forbester[1,2,3#], Mathew Clement[1], Dannielle Wellington[2,4], Amy Yeung[3,5], Sandra Dimonte[1], Morgan Marsden[1], Lucy Chapman[1], Eve L Coomber[3], Charlotte Tolley[3], Emily Lees[3], Christine Hale[3], Simon Clare[3], Irina Udalova[6], Tao Dong[2,4], Gordon Dougan[3,5], Ian R Humphreys[1]

Affiliations

1. Division of Infection and Immunity/Systems Immunity University Research Institute, Cardiff, UK
2. MRC Human Immunology Unit, MRC Weatherall Institute of Molecular Medicine, University of Oxford, Oxford, UK
3. Wellcome Trust Sanger Institute, Hinxton, Cambridge, UK
4. Chinese Academy of Medical Sciences Oxford Institute, Nuffield Department of Medicine, Oxford University, UK
5. Department of Medicine, University of Cambridge, Cambridge, UK
6. Kennedy Institute of Rheumatology, University of Oxford, Roosevelt Drive, Oxford, UK.

*Corresponding author

Email: forbesterJ@cardiff.ac.uk

Abstract

Recognition of Influenza A virus (IAV) by the innate immune system triggers pathways that restrict viral replication, activates innate immune cells, and regulates adaptive immunity. However, excessive innate immune activation can exaggerate disease. The pathways promoting excessive activation are incompletely understood, with limited experimental models to investigate mechanisms driving influenza-induced inflammation in humans. Interferon regulatory factor (IRF5) is a transcription factor that plays important roles in induction of cytokines after viral sensing. In an *in vivo* model of IAV infection, IRF5 deficiency reduced IAV-driven immune pathology and associated inflammatory cytokine production, specifically reducing cytokine-producing myeloid cell populations in *Irf5*$^{-/-}$ mice, but not impacting type 1 IFN production or virus replication. Using cytometry by time-of-flight (CyTOF), we identified that human lung IRF5 expression was highest in cells of the myeloid lineage. To investigate the role of IRF5 in mediating human inflammatory responses by myeloid cells to IAV, we employed human induced pluripotent stem cells (hIPSCs) with biallelic mutations in *IRF5*, demonstrating for the first time iPS-derived dendritic cells (iPS-DCs) with biallelic mutations can be used to investigate regulation of human virus-induced immune responses. Using this technology, we reveal that IRF5 deficiency in human DCs, or macrophages, corresponded with reduced virus-induced inflammatory cytokine production, with IRF5 acting downstream of TLR7 and, possibly, RIG-I after viral sensing. Thus, IRF5 acts as a regulator of myeloid cell inflammatory cytokine production during IAV infection in mice and humans, and drives immune-mediated viral pathogenesis independently of type 1 IFN and virus replication.

Journal of Virology JVI Journal of Virology

Importance

The inflammatory response to Influenza A virus (IAV) participates in infection control but contributes to disease severity. After viral detection intracellular pathways are activated, initiating cytokine production, but these pathways are incompletely understood. We show that interferon regulatory factor 5 (IRF5) mediates IAV-induced inflammation and, in mice, drives pathology. This was independent of antiviral type 1 IFN and virus replication, implying that IRF5 could be specifically targeted to treat influenza-induced inflammation. We show for the first time that human iPSC technology can be exploited in genetic studies of virus-induced immune responses. Using this technology, we deleted IRF5 in human myeloid cells. These IRF5-deficient cells exhibited impaired influenza-induced cytokine production and revealed that IRF5 acts downstream of Toll-like receptor 7 and possibly retinoic acid-inducible gene-I. Our data demonstrate the importance of IRF5 in influenza-induced inflammation, suggesting genetic variation in the IRF5 gene may influence host susceptibility to viral diseases.

Introduction

During infection with Influenza A virus (IAV), the host immune system must calibrate immune responses to control viral infection, whilst minimizing damage to host tissues. Disease manifestations are often associated with host inflammatory response to the virus (1, 2), and clinical outcome varies widely between individuals (3). The inflammatory response is initiated when pattern recognition receptors (PRRs) on innate immune cells recognize IAV pathogen-associated molecular patterns (PAMPs), which trigger signaling cascades resulting in the expression of specific inflammatory cytokines and chemokines (4, 5). Cytokines play various roles, such as directly inhibiting viral replication and activating the cytolytic

functions of T-cells, whereas chemokines recruit innate immune cells such as macrophages, neutrophils, NK cells and inflammatory monocytes to the lungs and airways (6).

Interferon regulatory factor 5 (IRF5) is a member of the IRF family of transcription factors, whose members have a shared N-terminal DNA binding domain and bind consensus interferon stimulated response element (ISRE) motifs. As ISREs are enriched in the regulatory regions of immune genes, IRFs play key roles as master regulators in the innate immune response (7), and may provide a mechanism for conferring signal specificity to target gene sets downstream of TLR signaling (8). Whilst IRF3 and IRF7 are necessary for induction of type I interferon (9, 10), IRF5 has been shown to be key in regulating inflammatory cytokine responses, generally acting downstream of TLR-MyD88 pathways (11, 12). Genetic polymorphisms in the IRF5 gene in humans have been linked to various autoimmune conditions including systemic lupus erythematosus, rheumatoid arthritis, Sjogren's syndrome, multiple sclerosis and inflammatory bowel disease (13). IRF5 has also been shown to be important in regulating immune responses to various pathogens in murine and human cell models (14–17). Additionally, *Irf5*$^{-/-}$ mice are resistant to systemic shock induced by CpG ligands and Lipopolysaccharide (LPS) (12). The extent to which IRF5 contributes to inflammation-induced pathologies, however, is unclear.

IRF5 is expressed predominantly by myeloid cells such as dendritic cells (DCs) and macrophages, in addition to B cells (13, 18). Myeloid cells can have protective and immune-pathogenic roles during IAV infection, producing inflammatory cytokines and initiating adaptive immune responses (19). Furthermore, inflammatory monocytes and monocyte-derived DCs have been identified to drive inflammation and lung pathology during IAV infection (19, 20).

Studying inflammatory cytokine responses in human myeloid cells is challenging. Human DCs are difficult to culture *in vitro* and, although DCs can be induced from blood-derived monocytes, these cells display morphological and functional differences to human primary DCs, for example differing in their capacity for T cell stimulation in comparison to $CD11c^{+}$ blood-derived DCs (21). Primary myeloid cells are also difficult to genetically manipulate, meaning that studies addressing the effect of host genetics on myeloid cell responses can be challenging. Human induced pluripotent stem cells (hIPSCs) offer a useful system for studying host-pathogen variation, because these cells are amenable to genetic manipulation, can be differentiated toward multiple cellular lineages and are self-renewing, allowing for production of sufficient quantities of cells of the same genetic background. hIPSC-derived macrophages (iPSDMs) have already been used to successfully model the interactions of pathogens with host cells (16, 22). However, to date, hIPSC technology has not been used to perform genetic investigations of virus-induced immune responses. To study the impact of IRF5 on human myeloid IAV-induced immune responses, we utilized hIPSCs generated from a healthy donor, or with mutations in *IRF5* generated by CRISPR/Cas9 engineering, differentiated into dendritic cells and macrophages as a human model system to assess the role of IRF5 in the regulation of immune responses to IAV. Using these tools in combination with studies of human lung cells, in addition to $Irf5^{-/-}$ mice, we show that IRF5 drives IAV-induced inflammatory cytokine responses in mice and humans without impacting virus replication and type 1 IFN secretion, and this process mediates viral pathogenesis *in vivo*.

Materials and Methods

Mice and viral infections

Irf5$^{-/-}$ mice were bred in-house on a C57BL/6 background and their generation has been described previously (12). C57BL/6 WT mice were purchased from Charles River or Envigo. Age- and sex-matched mice between 7 and 12 weeks of age were used in the experiments. Mice were infected intranasally with 3 x 10^3 PFU A/X-31 influenza in 50µl of sterile PBS. Mice weight was recorded daily and further monitored for signs of illness.

Plaque assays

Influenza from lungs of WT and *Irf5*$^{-/-}$ mice was quantified on Madin–Darby canine kidney (MDCK) cell monolayers after a 5-hour incubation at 37°C. Cell layers were then overlaid with methylcellulose (Sigma-Aldrich) and incubated at 37 °C for a further 48 hours. Media was then removed, and cell layers were washed, fixed and blocked and further incubated with anti-Influenza A nucleoprotein (Clone AA5H, Serotec) and then with anti-mouse IgG-HRP (BioRad). Plaques were developed using AEC peroxidase substrate solution and subsequently counted via light microscopy.

Leukocyte isolation, intracellular cytokine staining, and flow cytometry

BAL and lungs were collected from *Irf5*$^{-/-}$ and WT mice at days 2, 4 and 7 p.i. Lung digests were performed by incubation with collagenase solution (RPMI supplemented with 5% FBS, 1mg/ml collagenase D (Roche), 5 mM $CaCl_2$, 50 mg/mL DNAse I (Sigma-Aldrich)), and single cell suspensions were generated by passing through 100 µM filters. Cells were stained with Zombie Aqua™ fixable dye, incubated with anti-mouse CD16/CD32 (both BioLegend),

and stained for surface markers with a combination of the following antibodies (all BioLegend, BD Biosciences or Miltenyi Biotech). For murine myeloid panels cells were stained for surface markers: anti-mouse CD11b-FITC (M1/70, BioLegend), Ly6C-PerCP/Cy5.5 (HK1.4, BioLegend), Siglec F-PeVio770 (ES22-10D8, Miltenyi Biotec), CD64-Pe/Dazzle (X54-5/7.1, BioLegend), CD45R/B220-APC/Cy7 (RA3-6B2, BioLegend), MHC II-BV711 (M5/114.15.2, BioLegend), CD11c-BV605 (N418, BioLegend) and Siglec H-Pacific Blue (551, BioLegend). Following surface staining, some cells were fixed and permeabilized with Fixation/Permeabilization solution (BD Biosciences) and stained with anti–IL-6-PE (MP5-20F3; BioLegend) and TNF-α-APC (MP6-XT22, BioLegend). All data was acquired using an Attune NxT flow cytometer (Thermo Fisher Scientific). Electronic compensation was performed with Ab capture beads stained separately with individual mAbs used in the experimental panel. Data were analyzed using FlowJo software (TreeStar Inc). Total numbers of different cell populations were calculated by multiplying the total number of viable leukocytes (assessed by trypan blue exclusion) by the percentage of positive cells, as detected by flow cytometry.

Mass Cytometry staining for IRF5 expression

Para-tumor lung tissue samples from metastatic cancer or fibrosis patients were extracted and deemed to show no visible signs of inflammation by a pathologist. PBMC from one donor were run with each lung sample to control for inter-run variability. 100 mL of heparinized blood was drawn from a healthy control donor, PBMCs were isolated and aliquots were frozen until use. Directly conjugated antibodies (CD45-89Y, clone HI30; EpCAM-141Pr, clone 9C4; CD31-151Eu, clone EPR3094; CD68-159Tb, clone KP1; Siglec 8-164Dy, clone 7C9) were all purchased from Fluidigm. Conjugations for other antibodies (CD11b-142Nd, clone ICRF44; CD4-145Nd, clone RPA-T4; CD20-147Sm, clone 2H7; CD115-152Sm, clone

12-3A3-1810; CD123-155Gd, clone 6H6; CD14-160Gd, clone M5P2; CD56-166Er, clone NCM/HCD56; CD8-168Er, clone SK1; HLA-DR-169Tm, clone L243; CD3-170Er, clone UCHT1; CD1c-171Yb, clone L161; CD141-173Yb, clone M80) were performed with the Maxpar X8 Multi-Metal Labeling Kit (Fluidigm) according to the manufacturer's instructions.

Cells re-suspended at 1×10^7 cells/mL were stained with 5 mmol/L Cisplatin (Fluidigm; live/dead) and surface antibody cocktail before permeabilization with Maxpar nuclear antigen staining buffer and staining with anti-IRF5 (Conjugate, 175Lu; clone, EPR17067). An un-permeabilized control was treated with cell staining buffer and stained with intracellular antibodies. Cells were stained with 125 nM Ir-Intercalator (Fluidigm) according to Fluidigm protocols and fixed with 1.6% formaldehyde. Cells were counted on a BD Accuri C6, and resuspended at 2×10^6 cells/mL in 0.1×EQ Four Element Calibration Beads (Fluidigm). Cells were acquired using a CyTOF Helios cytometer (Fluidigm). Data was processed and normalized using the CyTOF software v6.7 (Fluidigm). Data was analyzed using FlowJo (Treestar Inc).

Mass cytometry Analysis

CyTOF data were analyzed using FlowJo 10.5.2 (TreeStar Inc). After gating on live, intact, singlet cells, CD45 v EpCAM expression was used to identify epithelial cells ($CD45^-$ $EpCAM^+$) or immune cells ($CD45^+EpCAM^-$). $CD45^+EpCAM^-$ cells were down-sampled to maximum 200,000 per sample, with stained and control samples were concatenated into one file. The concatenated file was run through a UMAP analysis of the surface markers CD11b, CD4, CD20, CD123, CD68, CD14, Siglec 8, CD56, CD8, HLA-DR, CD3, CD1c, CD141, CD16. Post-UMAP analysis, distinct cell subsets were identified by mapping expression of

specific subset markers back onto the UMAP to define populations of immune cells. Subsets were defined as follows: $CD4^+$ T cells, $CD3^+CD4^+CD20^-$; $CD8^+$ T cells, $CD3^+CD20^-CD8^+$; B cells, $CD3^-CD20^+$; NK cells, $CD3^-CD20^-CD56^+$; $CD14^+$ Monocytes, $CD16^-$ $CD11b^+CD14^+HLA\text{-}DR^+$; $CD16^+$ Monocytes, $CD14^-CD11b^+CD16^+HLA\text{-}DR^+$; Macrophages, $CD11b^+CD68^+HLA\text{-}DR^+$; pDCs, $CD123^+CD11b^+HLA\text{-}DR^+$; $CD141^+$ cDCs, $CD11b^+HLA\text{-}DR^+CD1c^-CD141^+$; $CD1c^+$ cDCs, $CD11b^+HLA\text{-}DR^+CD1c^+CD141^-$; Eosinophils, $Siglec8^+$CD123-; Basophils, $Siglec8^+CD123^+$; Epithelial cells, $CD45^-$ $EpCAM^+$. Individual samples were identified by gating on event length v sample ID, and the median value was determined for IRF5 for each individual sample.

Generation of blood-derived human dendritic cells

PBMCs from three independent donors were isolated from leukapheresis products using Lymphoprep density gradient centrifugation and SepMate PBMC isolation tubes (StemCell Technologies), under the Weatherall Institute of Molecular Medicine, University of Oxford Human Tissue Authority License (12433). Human CD14 microbeads were used in combination with LS columns (both Miltenyi Biotec) to positively select $CD14^+$ blood monocytes. $CD14^+$ cells were seeded at a density $3\text{-}5\times10^6$ isolated monocytes in 3 mL of RPMI media supplemented with 10% heat inactivated Fetal Bovine Serum (FBS; Sigma-Aldrich), 250 IU/mL IL-4 and 800 IU/mL GM-CSF into a 6-well plate and incubated at 37°C for 2 days. After 2 days 1.5ml of medium was removed from each well, and 1.5 mL of fresh medium supplemented with 500 IU/mL IL-4 and 1600 IU/mL GM-CSF was added. After a further 3-day incubation, cells were harvested at the immature phenotype and assayed, or further matured with LPS at 10 μg/mL for 24 hours.

224 **hIPSCs**

225 The healthy control hIPSC line Kolf2 was acquired through the Human Induced Pluripotent
226 Stem Cells Initiative Consortium (HipSci; www.hipsci.org), through which it was also
227 characterized (23). Generation of IRF5$^{-/-}$ iPSCs has been previously described (16). Briefly,
228 Kolf2 iPSCs were dissociated to single cells and nucleofected (Amaxa2b nucleofector,
229 LONZA) with Cas9 coding plasmid (hCas9, Addgene 41815), sgRNA plasmid (left
230 CRISPR_IRF5 CCAAGTGGAAGGCCAACCTGCGC; right CRISPR_IRF5
231 GACTTCCGCCTCATCTACGACGG) and donor plasmid, containing 5' and 3' homology
232 arms for IRF5 targeting and pL1-EF1αPuro-L2 cassette. Post nucleofection, cells were
233 selected for up to 11 days with 0.25 μg/mL puromycin, after which individual colonies were
234 picked onto 96-well plates, grown to confluence and then replica plated. To genotype
235 individual clones from a 96-well replica plates, cells were lysed and used for PCR
236 amplification with LongAmp Taq DNA Polymerase (NEB). Insertion of the cassette into the
237 correct locus was confirmed by visualizing on 1% E-gel (Life Tech.) PCR products were
238 generated by gene specific and cassette specific primers, with single integration of cassette
239 confirmed by a qPCR copy number assay. Positive clones were then screened for damage to
240 the non-targeted allele via PCR and Sanger sequencing. To generate our complemented IRF5
241 iPSC line (IRF5^{Comp}) and restore expression of functional IRF5 in the IRF5$^{-/-}$ iPSCs, we
242 generated the AAVS1 EF1a-IRF5-PGK-puro targeting vector by Gibson assembly. The
243 Gibson assembly product was transformed into OneShot TOP10 chemically competent *E.*
244 *coli* (Thermo Fisher Scientific) and positive colonies were picked. Isolated plasmids from the
245 positive colonies were taken to confirm the presence and sequence of EF1α-IRF5 in the
246 targeting vector by restriction digests, PCR and sequencing. Subsequently, the targeting
247 vector was transformed into competent *E. coli* to isolate endotoxin-free plasmids to transform
248 into the IRF5$^{-/-}$ iPSCs. We transfected the mutant human hIPSCs with TALEN-L

(CCCCTCCACCCCACAGT), TALEN-R (AGGATTGGTGACAGAAA) and targeting vector via nucleofection (Amaxa Biosystems). The resultant targeted cells were selected on puromycin for 7 days and the surviving colonies were picked and expanded. The positive clones were confirmed by RT-qPCR for *IRF5* expression and flow cytometry for protein expression. Prior to differentiation, iPSCs were grown feeder-free using the Essential 8 Flex Medium kit (Thermo Fisher Scientific) on Vitronectin (VTN-N, Thermo Fisher Scientific) coated plates as per manufacturer's instructions to 70-80% confluency. iPSCs were harvested for differentiation using Versene solution (Thermo Fisher Scientific).

Differentiation of iPSCs to dendritic cells and macrophages

To differentiate iPSCs to dendritic cells slight modifications were made to a previously published protocol (24). Briefly, upon reaching confluency iPSCs were harvested and plated into Essential 8 Flex medium supplemented with 50 ng/mL BMP-4 (Bio-Techne), 20 ng/mL SCF (Bio-Techne), 50 ng/mL VEGF (Peprotech EC Ltd.), and 50ng/mL GM-CSF (Peprotech EC Ltd.) in ultra-low attachment plates (Corning). Media was changed to X-VIVO-15 (Lonza), with sequential removal of BMP-4 by day 5, VEGF by approximately day 14 and SCF by approximately day 19. In addition, IL-4 (Peprotech EC Ltd.) was added sequentially in increasing concentrations, starting from approximately day 12 at 25 ng/mL and increasing to 100 ng/mL by approximately day 20. By day 20, floating immature DCs were harvested from ULA plates, filtered through 70μM filters (Corning), counted and seeded at 1 x 10^6 per well of 6 well CellBind plates (Corning) in X-VIVO-15 media supplemented with 100 ng/mL IL-4 and 50 ng/mL GM-CSF. iPS-DCs were used for assays at the immature phase between 4-5 days post seeding in CellBind plates. In addition, iPS-DCs could be matured for a further 48 hours 5 days post plating, by addition of 50 ng/ml of GM-CSF, 100 ng/ml IL-4, 20 ng/ml IFNγ (Bio-Techne), 50 ng/ml TNFα (Bio-Techne), 10 ng/ml IL-1β (Bio-Techne) and 1 μg/ml

PGE_2 (Sigma-Aldrich), to induce further expression of $CD141^+$ DC lineage markers. For assays, floating iPS-DCs were harvested from differentiation plates, washed with PBS, counted and seeded in X-VIVO-15 media without cytokines at an assay dependent concentration. To differentiate iPSCs to macrophages, the approach of Hale et al (22) and van Wilgenburg et al (25) was modified to allow for feeder-free differentiation. Briefly, upon reaching confluency, human iPSCs were collected and transferred into Essential 8 Flex medium supplemented with 50 ng/mL BMP-4 (Bio-Techne), 20 ng/mL SCF (Bio-Techne) and 50 ng/mL VEGF (Peprotech EC Ltd.) in ultra-low attachment plates (Corning) for 4 days to generate Embryoid Bodies (EBs). On day 5, EBs were used for generation of myeloid precursor cells by plating into 6-well tissue culture treated plates (Corning) coated for two hours at room temperature with 0.1% gelatin, in X-VIVO-15 media supplemented with 25 ng/mL IL-3 (Bio-Techne) and 50 ng/mL M-CSF (Bio-Techne). After several weeks, floating myeloid precursors were harvested and terminally differentiated into matured macrophages (iPSDMs) in the presence of higher concentrations of M-CSF (100 ng/mL) for 7 days. For experiments, macrophages were detached using Lidocaine solution (4 mg/mL lidocaine-HCl with 10 mM EDTA in PBS), and seeded at 2×10^5 cells per well (24-well plate) or 1×10^6 cells per well (six-well plate).

Preparation of RNA and RT-qPCR

iPS-DCs were harvested from plates and RNA was prepared using the RNeasy minikit (Qiagen). RNA was reverse transcribed with the QuantiTect reverse transcription (RT) kit (Qiagen) according to the manufacturer's protocol. All RT-qPCR experiments were performed with TaqMan gene expression assays and TaqMan gene expression master mix (Applied Biosystems) on the Applied Biosystems StepOne real-time PCR system. RT-qPCR

data were analyzed via the comparative CT method with glyceraldehyde 3-phosphate dehydrogenase (GAPDH) as an endogenous control.

Flow cytometric analysis of iPS-DCs

For analysis of surface markers on iPS-DCs, cells were stained with Zombie Aqua™ fixable dye (BioLegend), Fc receptors were blocked using Human TruStain FcX (BioLegend) and cells were then subsequently stained for surface markers with a combination of the following antibodies: anti-human HLA-DR-AlexaFluor488 (AF488) (L243, BioLegend) or CD14-FITC (M5E2, BioLegend), CD83-PerCP/Cy5.5 (HB15e, BioLegend) or CD1c-PerCP/Cy5.5 (L161, BioLegend), CD141-PE/Cy7 (M80, BioLegend) or DC-SIGN-PE/Cy7 (9E9A8, BioLegend), or XCR1-PE (FAB8571, Bio-Techne), CD11c-APC/Cy7 (Bu15, BioLegend), CLEC9A-APC (8F9, BioLegend), CD86-BV711 (IT2.2, BioLegend), CD303-BV785 (201A, BioLegend) or HLA-DR-BV785 (L243, BioLegend), or HLA-A,B,C-Pacific Blue (W6/32, BioLegend). For detection of IRF5 or IAV nucleoprotein, cells were stained with Zombie Aqua™ fixable dye, fixed with 4% Paraformaldehyde and permeabilized with 0.5% Triton X, followed by incubation with Human TruStain FcX and staining with IRF5-AF647 (EPR6094, Abcam) or Anti-Influenza A Virus Nucleoprotein antibody (431, Abcam) in 0.1% Triton X solution. All data was acquired using a BD LSRFortessa flow cytometer (BD Biosciences). Electronic compensation was performed with Ab capture beads stained separately with individual mAbs used in the experimental panel. Data were analyzed using FlowJo software (TreeStar Inc).

Infection of iPS-DCs and iPSDMs with IAV

iPS-DCs, iPSDMs or human moDCs were infected with A/X-31 influenza at an MOI of 1 by addition of virus to culture supernatant and centrifugation at 630 g for 20 minutes at room temperature, after which media was replaced with fresh culture medium.

Immunostaining for confocal microscopy

iPS-DCs were harvested from plates and spun onto slides coated with 0.01% Poly-l-Lysine using a Cytospin cytocentrifuge. Samples were blocked and permeabilized in 2% Triton X-100 (Sigma-Aldrich) in 5% FBS diluted in PBS. Primary antibodies were applied at room temperature in 0.25% Triton X-100 in 5% FBS diluted in PBS for 1 hour and then rinsed 3 times with PBS. Secondary antibodies were applied in the same manner. Nuclei were counterstained with 10 nM DAPI dilactate diluted in PBS for 30 min, samples were rinsed 6 times with PBS, and then mounted in Prolong-Gold with added DAPI (Invitrogen) and analyzed using a Leica SP8 DLS (Digital light sheet) microscope.

TLR/RIG-I stimulations

iPS-DCs were plated at 1 x 10^4 cells per well in 200ul of X-VIVO-15 media without cytokines. TLR ligands were added directly to the media, and supernatants were harvested after 24-hour incubation at 37°C. For assays TLR ligands were used at the following concentrations: Pam3CSK4 (300 ng/mL; InvivoGen), Poly I:C (50 μg/mL; InvivoGen), Lipopolysaccharide (500 ng/mL; Sigma-Aldrich), Imiquimod (50 μg/mL; InvivoGen); ODN 2216 (3 μg/mL; Miltenyi Biotech). For RIG-I stimulation 1 μg of 3p-hpRNA was complexed with LyoVec (InvivoGen) for 15 minutes at room temperature and then added to iPS-DCs at 10 ng/mL.

Cytokine and chemokine analysis

Human IL-6 and TNF-α protein was measured by ELISA (BioLegend). ELISAs for human IFN-α and IFN-β were performed on supernatants harvested from mock infected and IAV infected iPS-DCs using the Verikine Human Interferon Alpha/Interferon Beta ELISA kit (PBL Assay Science). Murine BAL cytokines were detected using the LEGENDPlex mouse

inflammation panel (13-plex; BioLegend) as per the manufacturer's instructions at 2, 4 and 6 days p.i. and analyzed using the LEGENDPlex analysis software. ELISAs for mouse IFN-α and IFN-β were performed on BAL from naïve mice and mice 2 days p.i using VeriKine Mouse Interferon Alpha/Interferon Beta ELISA Kits (PBL Assay Science).

Blocking assays

For blocking assays cells were either pre-incubated for 1 hour with inhibitor (IMD 0354; IKKβ inhibitor, (Santa Cruz Biotechnology) 5 μg/mL)) or inhibitor was added directly with viral inoculum (TLR7 inhibitor, ODN 20958, Miltenyi Biotech, 5 μM). For type I IFN blocking, cells were pre-incubated with 5 μg/mL anti-IFNAR1 antibody (Sigma-Aldrich) for 1 hour prior to infection with A/X-31 influenza without removal of antibody.

Statistical analysis

Statistical significance was performed with GraphPad Prism software. Mann Whitney-U or Student's *t*-tests were used for two-group comparisons. For comparison of IRF5 expression between lung cell subsets identified via CyTOF a repeated measurement one-way ANOVA was used. A p value of ≤ 0.05 was considered to be significant. For all tests performed, p values are reported as n.s. > 0.05; * ≤ 0.05; ** ≤ 0.01; *** ≤ 0.001; **** ≤ 0.0001

Ethics statement

All animal studies were performed at Cardiff University (Heath Park research support facility) under UK Home Office Project License number (P7867DADD), as approved by the UK Home Office, London, United Kingdom. Written consent was obtained for the use of cell lines for the HIPSCI project from healthy volunteers. A favorable ethical opinion was granted by the National Research Ethics Service (NRES) Research Ethics Committee Yorkshire and

The Humber – Leeds West, reference number 15/YH/0391. Lung tissue samples were obtained from lung cancer and fibrosis patients from Oxford Radcliffe Biobank with written consent: a favorable ethical opinion was granted by the South Central-Oxford C Research Ethics Committee for collection and frozen storage of both tumor and para-tumor lung samples (Reference number: 09/H0606/5+5).

Results

IRF5 mediates inflammatory cytokine and myeloid cell responses to Influenza A virus infection in mice

The mouse is the primary experimental model for studying immunological response to IAV, where it has been demonstrated that excessive inflammatory cytokine and cellular immune responses promote lung pathology (2, 26, 27). We first used this model to assess whether IRF5 impacts influenza-induced immune responses during IAV infection *in vivo*, using the low pathogenicity murine-adapted H3N2 Influenza A virus (A/X-31). Prior studies have indicated that viral infections of *Irf5*$^{-/-}$ mice lead to reduced cytokine production in comparison to wild type (WT) controls (14, 17, 28). In accordance, we observed a significant reduction in early cytokine release in *Irf5*$^{-/-}$ mice, with IL-23, IFN-γ, TNF-α, MCP-1, IL-6, IL-17A, IL-1α, IL-12p70, GM-CSF, IL-1β and IL-27 all significantly reduced in the Bronchoalveolar Lavage (BAL) of *Irf5*$^{-/-}$ mice in comparison to WT controls 2 days post-infection (p.i) (Fig. 1A), with some cytokines remaining significantly reduced in *Irf5*$^{-/-}$ mice 4 days p.i (Fig. 1A). In contrast to other viral infections (17), IFN-α or IFN-β production in response to influenza infection were unaltered (Fig. 1B) at a time-point (day 2 p.i) previously demonstrated to represent the time of significant A/X-31 influenza-induced type 1 IFN secretion in this model (29). These data therefore imply that IRF5 selectively modulates

expression of certain influenza-induced inflammatory cytokines independently of type I IFNs in mice.

Early reduction in inflammatory cytokine production in *Irf5*$^{-/-}$ mice was accompanied by a moderate amelioration of IAV-induced weight loss (Fig. 2A). Interestingly, a recent study reported that reduced IAV-induced cytokine production in *Irf5*$^{-/-}$ mice was associated with reduced virus replication (28). However, at a time-point where we observed substantially reduced cytokine production (day 2 p.i), we observed no alteration in IAV load in *Irf5*$^{-/-}$ mice (Fig. 2B), nor did we observe altered virus load in *Irf5*$^{-/-}$ mice at a later timepoint of 4 days p.i (Fig. 2B). Thus, our data demonstrates for the first time that IRF5 promotes IAV-induced weight loss independently of an impact on influenza replication.

Given the established role for myeloid cells in pulmonary inflammation during IAV infection (30, 31), we used polychromatic flow cytometry panels to assess whether Irf5 influenced myeloid cell accumulation during infection. Reductions in monocyte-derived DCs, interstitial macrophages, inflammatory monocytes and conventional DCs in the lungs of *Irf5*$^{-/-}$ mice were observed at 2 days p.i (Fig. 2C). Importantly, lower cytokine responses in *Irf5*$^{-/-}$ mice were accompanied by significant reductions in IL-6^{+} cDCs and TNF-α^{+} cDCs, interstitial macrophages, cDCs and pDCs in the airways (Fig. 2D). Thus, these data suggested that Irf5 plays a key role in shaping the early innate inflammatory response during influenza infection and point to a central role for myeloid cells in promoting IRF5-driven viral disease.

Myeloid cells in human lung express high levels of IRF5

Although the mouse is a useful model for probing immune responses to IAV, numerous differences exist between the mouse and human immune system. It was therefore important

423 to investigate the role of human IRF5 in IAV-induced immune responses. We first measured
424 IRF5 expression in multiple cell subsets in human lung samples using CyTOF (Fig. 3A).
425 Using lung samples from four independent donors, we identified significantly different IRF5
426 expression dependent on cell subset ($p = 0.0252$, R-Square = 0.9098) (Fig. 3B), with cells of
427 the myeloid lineage, particularly eosinophils, basophils and monocytes, displaying highest
428 expression of IRF5 in human lung. Expression was higher in $CD1c^+$ DCs and $CD141^+$ DCs
429 than in lung resident macrophages, where expression was relatively low. Furthermore, when
430 IRF5 expression data was combined for all myeloid cell subsets and all lymphoid cell subsets
431 (Fig. 3C), expression of IRF5 was significantly higher in myeloid cells in comparison to
432 lymphoid cells (median expression myeloid = 6.01, median expression lymphoid = 1.79; $p =$
433 <0.0001), suggesting that IRF5 expression is highest in the myeloid compartment.
434
435 **iPSCs with a biallelic mutation in *IRF5* can be differentiated into conventional dendritic**
436 **cells**
437 Given that, in the human lung, IRF5 expression was highest in cells of the myeloid lineage
438 and that in mice Irf5 promoted pro-inflammatory cytokine production by myeloid cells in
439 response to IAV infection, we next sought to establish a human myeloid cell model to
440 scrutinize the role of IRF5 in myeloid cell cytokine response to IAV. We differentiated a
441 hIPSC line with a biallelic mutation in IRF5 generated using CRISPR/Cas9 genome editing
442 (16) and the parental line Kolf2, into iPS-DCs using a published differentiation strategy (24).
443 We also generated a complemented isogenic control line for $IRF5^{-/-}$ (hereafter "$IRF5^{Comp}$") to
444 confirm IRF5-dependency of any phenotypes observed (32). To confirm gene editing
445 strategies, we examined the expression of IRF5 in Kolf2, $IRF5^{-/-}$ and $IRF5^{Comp}$ iPS-DCs.
446 *IRF5* mRNA was detected in Kolf2 iPS-DCs but not $IRF5^{-/-}$ iPS-DCs, with expression
447 restored in $IRF5^{Comp}$ iPS-DCs (Fig. 4A). Similar restoration of IRF5 protein expression in

448 IRF5^{Comp} iPS-DCs was observed (Fig. 4B). Furthermore, after infection of iPS-DCs with
449 IAV, IRF5 was detected in Kolf2 iPS-DCs and not IRF5$^{-/-}$ iPS-DCs by immunostaining (Fig.
450 4C). We then compared IAV-induced cytokine production by iPS-DCs from our healthy
451 control iPSC line Kolf2 with monocyte-derived DCs from the blood of three healthy donors
452 which were left either immature or matured for 48 hours with LPS. iPS-DCs demonstrated
453 similar cytokine profiles after IAV infection to immature monocyte-derived DCs (Fig. 4D),
454 validating iPS-DCs as an experimental system for examining virus-induced cytokine
455 responses.
456
457 It has previously been shown that IRF5 deficiency or TALEN-based engineering targeting
458 the AAVS1 viral integration site does not affect the differentiation capacity of iPSCs to iPS-
459 derived macrophages (iPSDMs) (16, 33). To ensure that genome editing strategies had not
460 altered the differentiation capacity of iPSCs to dendritic cells, we assessed the differentiation
461 efficiency of Kolf2, IRF5$^{-/-}$ and IRF5^{Comp} iPSCs. We observed similar numbers of cells
462 harvested from embryoid bodies (EBs) from day 19-24 of differentiation, with no significant
463 difference in the number of cells harvested from eight independent differentiations per line
464 (Fig. 5A). After completion of the 25-day DC differentiation, DC marker expression was
465 examined by flow cytometry, with CD141, CLEC9A, CD11c, MHC II and CD86 similarly
466 expressed in all three iPS-DC lines (Fig. 5B). There are three main subsets of human DCs,
467 pDCs and two subsets of myeloid (conventional) DCs, CD1c^{+} and CD141^{+}, with DC
468 hematopoiesis distinct from the development of monocytes (34). iPS-DCs express markers
469 of human conventional DCs including CD11c and CD141 (Fig. 5B), as well as HLA-DR,
470 CD86 and CLEC9A, which have been shown to be expressed by human CD141^{+} DCs (35).
471 We did not detect CD303 expression, a marker for pDCs or CD1c, the marker for the other
472 subset of human conventional dendritic cells (36). As observed by Sachamitr et al (24) we

also detected CD14 and DC-SIGN expression by iPS-DCs (Forbester J & Humphreys I, unpublished data). Gene expression analysis confirmed similar induction of the DC markers *CD83* and *CD86* in all three iPSC lines after differentiation to iPS-DCs, and loss of expression of the pluripotency markers *NANOG* and *POU5F1* (Fig. 5C). Morphology of Kolf2, IRF5$^{-/-}$ and IRF5^{Comp} iPS-DCs in culture was indistinguishable (Fig. 5D). Taken together, these data suggest that neither IRF5 deficiency nor TALEN-based engineering influence iPSC differentiation.

IRF5 enhances IAV-induced inflammatory cytokine production in iPS-DCs

After confirming that IRF5 deficiency did not alter iPS-DC surface phenotype or morphology (Fig. 5) and that iPS-DCs exhibit similar cytokine profiles to human monocyte-derived DCs after IAV stimulation (Fig. 4D), we next used iPS-DCs to determine whether IRF5 has a cell-intrinsic role in human DC cytokine production, in particular the pro-inflammatory cytokines IL-6 and TNF-α. Despite a protective role for IL-6 being reported in murine models of IAV infection (37, 38), high production of IL-6 is linked to severity of symptoms in humans patient cohorts (39, 40), whereas TNF-α has been shown to enhance cellular inflammation and pathology during IAV infection (26).

24 hours after stimulation of iPS-DCs with IAV, IL-6 and TNF-α production by IRF5$^{-/-}$ iPS-DCs was significantly reduced in comparison to Kolf2 iPS-DCs whereas cytokine production was restored in IRF5^{Comp} iPS-DCs (Fig. 6A, iPS-DCs). IRF5 deficiency had no impact on virus entry, as indicated by comparable influenza nucleoprotein (NP) staining after 24 hours (Fig. 6B & C). In addition, there was no significant difference in cell viability after IAV stimulation, as measured by live viability dye and flow cytometry 24h p.i. (Mean ± SEM % live cells: IRF5^{Comp}, 65.767 ± 0.353; IRF5$^{-/-}$, 63.95 ± 1.655; Kolf2, 70 ± 1.654). Surface

analysis of DC markers by flow cytometry showed that the number of iPS-DCs expressing DC maturation markers after IAV infection was similarly significantly increased in Kolf2, IRF5$^{-/-}$ and IRF5^{Comp} iPS-DCs (Fig. 6D). Moreover, gene complementation has previously been used to inhibit immune responsiveness in the context of restoration of expression of the inhibitory IL-10 receptor into *IL10RB*$^{-/-}$ iPS-derived myeloid cells (33). Thus we do not believe that restored cytokine responsivess of complemented IRF5$^{-/-}$ cells is a consequence of non-specific induction of cytokine secretion by the complementation process, but instead is due to IRF5 itself. Collectively, these data suggest that IRF5 deficiency selectively alters iPS-DC cytokine production after exposure to IAV. In addition, to probe IRF5 deficiency in a different myeloid cell lineage, we differentiated IRF5$^{-/-}$, Kolf2 and IRF5^{Comp} iPSCs to macrophages (iPSDMs) using a slightly modified version of a previously published protocol (22), demonstrating a similar significant reduction in IL-6 and TNF-α production as observed in iPS-DCs (Fig. 6A, iPSDMs).

IRF5 acts downstream of TLR7 and, possibly, RIG-I signalling pathways to drive human myeloid cell cytokine responses to IAV

In some experimental systems, IRF5 mediates virus-induced production of type I IFN (17, 41). Given that type I IFN is implicated in driving influenza-induced inflammatory cytokine responses (42), we assessed whether IRF5 deficiency impacted influenza-induced IFN production. Blocking type I IFN reduced IAV-induced IL-6 and TNF-α production albeit, in the case of IL-6, not to levels produced by IRF5$^{-/-}$ iPS-DCs (Fig. 7A). Furthermore, IRF5 had no impact on type I IFN secretion by iPS-DCs (Fig. 7B). Thus, although type I IFN enhanced IRF5-induced pro-inflammatory cytokine secretion, the production of type I IFN by iPS-DCs was not an IRF5-regulated process.

We next investigated which PRRs require IRF5 to elicit cytokine responses following IAV stimulation of iPS-DCs. IAV is detected by endosomal TLR7, and members of the DExDC helicase family and RIG-I in dendritic cells (43–45). Consistent with data from human and murine macrophages (12, 46), IRF5$^{-/-}$ iPS-DCs produced significantly less IL-6 in response to agonists of TLR7 (and TLRs 4, 3 and 9, Fig. 8A). Moreover, stimulation of IRF5$^{-/-}$ iPS-DCs with the RIG-I-specific agonist 3p-hpRNA led to a significant reduction in IL-6 production (Fig. 8B), demonstrating that IRF5 mediates RIG-I- and TLR7-induced responses in iPS-DCs. Substantial IFN-dependent induction of the RIG-I encoding gene *DDX58* and, to a lesser extent, *TLR7* were observed upon IAV stimulation of iPS-DCs (Fig. 8C & D), and IRF5 deficiency did not impair baseline PRR expression (Fig. 8E), suggesting that reduced expression of pro-inflammatory cytokines in response to TLR7, RIG-I and IAV stimulation in IRF5$^{-/-}$ iPS-DCs was not a consequence of restricted PRR expression by these cells.

Finally, we wanted to determine which PRRs mediated IAV-induced cytokine responses in iPS-DCs. Because 1) there is no selective antagonist of RIG-I and 2) human CD141^{+} DCs express TLR7 (47), we focused on the role of TLR7 in mediating IAV-induced iPS-DC cytokine responses. Addition of the specific TLR7 antagonist ODN 20958 to IAV-stimulated Kolf2 iPS-DCs significantly abated IL-6 production whereas TLR7 inhibition in IRF5$^{-/-}$ iPS-DCs did not further reduce IAV-induced IL-6 responses (Fig. 8F). These data suggest that IRF5 promotes TLR7 mediated cytokine responses following IAV detection by human DCs. However, IAV-induced cytokine secretion was incompletely inhibited by TLR7 blockade in Kolf2 iPS-DCs, suggesting that other PRRs contribute to IRF5-mediated responses. IKKβ has been shown to play a crucial role in IRF5 and NF-κB activation (11). In support of this, pre-treatment of IAV-stimulated iPC-DCs with the IKKβ inhibitor IMD 0354 dramatically reduced IAV-induced cytokine production by iPS-DCs (Fig. 8B) implying that other PRRs

548 including, possibly, RIG-I contribute to IAV-induced cytokine responses by iPS-DCs in
549 addition to TLR7.
550
551 **Discussion**
552 Here, using iPS-DCs as a model system, we have shown that IRF5 expression by myeloid
553 cells is important in driving the inflammatory response to IAV, without impacting viral
554 uptake by iPS-DCs or DC maturation. Using various blocking assays and stimulation with
555 TLR/RLR ligands, we show that IRF5 is most likely acting downstream of TLR7 and,
556 possibly, RIG-I signaling to drive the production of pro-inflammatory cytokines.
557
558 Given that IFN-stimulated genes contribute to anti-influenza immunity (48), to identify
559 whether IFR5 and/or related pathways could be safely exploited to dampen inflammatory
560 cytokine responses to influenza it is important to understand the relationship between IRF5
561 and virus-induced type 1 IFN. We found that IRF5$^{-/-}$ iPS-DCs and *Irf5*$^{-/-}$ mice were not
562 deficient in type I IFN production, but that type I IFN enhances the IRF5-mediated
563 inflammatory cytokine response, a process associated with IFN-mediated induction of TLR7
564 and RIG-I. Although certain studies have reported a role for IRF5 in type I IFN induction
565 directly in certain contexts (28, 46, 49) functional redundancy between IRF proteins may
566 exist [46]. Also, although a role for IRF5 in promoting type 1 IFN secretion following
567 influenza infection *in vivo* has been reported, the same studies observed reduced virus
568 replication in *Irf5*$^{-/-}$ mice, precluding the possibility to uncouple decreased virus replication
569 and subsequent pattern recognition receptor stimulation from a direct influence of IRF5 on
570 type 1 IFN expression. Furthermore, early *in vivo* studies of Irf5 responses to viruses may
571 have been confounded by a *Dock2* mutation prevalent in *Irf5*$^{-/-}$ mouse colonies (50). Also, it
572 has been demonstrated *in vitro* that, unlike IRF3 and IRF7, IRF5 does not bind to the virus-

response elements in IFN promotors (51). IRF5-mediated induction of type I IFN may also be virus-specific, at least *in vitro*, with NDV, VSV and HSV-1 infection shown to activate IRF5 but lead to induction of distinct IFNA gene subtypes in human cell lines (52). IRF3 and IRF7 are activated by IAV, and these transcription factors have been shown to be necessary for inducing type I IFN after IAV infection (53, 54). Therefore, we suggest that after sensing of IAV by dendritic cells, IRF3, IRF5, and IRF7 are induced, resulting in the production of type I IFN and inflammatory cytokines, with the type I IFN induced by IRF3 and IRF7 exacerbating IRF5 activation, likely in part through induction of TLR7 and, possibly, RIG-I expression. In the context of influenza pathogenesis, our data imply that IRF5 could be safely targeted to limit virus-induced pro-inflammatory cytokine production without affecting IFN production and associated induction of antiviral effector genes.

The phenotype of reduced inflammatory cytokines observed in our iPS-DC model was also evident *in vivo* using *Irf5*$^{-/-}$ mice. Although we observed no mortality in either WT or *Irf5*$^{-/-}$ mice (Forbester J & Humphreys I, unpublished data), we observed reduced cytokine production by myeloid cells that correlated with reduced cellular pulmonary infiltration and a moderate impact on virus-induced weight loss. Although *Irf5*$^{-/-}$ mice have previously been shown to be less susceptible to IAV-induced pathology (28), in this study we were able to de-couple viral load and inflammatory cytokines in the early stages of infection, demonstrating that the enhanced pathology in WT compared to *Irf5*$^{-/-}$ mice was immune-mediated rather than a consequence of heightened virus replication. Why differences exist between our data and those obtained by Chen *et al* (28) is unclear, although this may reflect the different influenza strains (H3N2 versus H1N1) used in these experiments. Irrespective, the data presented herein demonstrates that IRF5 modulates viral pathogenesis via the regulation of inflammation and not virus replication, and that targeting this pathway as an adjunct therapy

598 to antiviral drug treatment may represent an effective therapeutic approach to treatment of
599 influenza pathogenesis.
600
601 Although the mouse provides a useful model to study viral pathogenesis there are inherent
602 immunological differences between mice and humans (55). Therefore, we wanted to establish
603 a human cell system amenable to genetic manipulation, so that gene function can be
604 understood in the context of a human cellular environment. Given that primary human
605 myeloid cells are difficult to genetically manipulate and access in large numbers, hIPSCs
606 offer a solution; once hIPSCs are generated they can be differentiated down multiple cellular
607 lineages, providing the opportunity to study gene function in multiple different cell types,
608 with a defined genetic background. In addition, as hIPSCs are self-renewing, starting material
609 is an unlimited resource. Furthermore, many research groups have shown that hIPSCs can be
610 relatively easily genetically manipulated using tools such as Zinc finger nucleases, TALENs
611 and CRISPR-Cas9 systems (56). Here, we show that iPSCs can be differentiated into DCs
612 expressing markers of human $CD141^+$ myeloid DCs. However, the levels of the specific
613 lineage markers for $CD141^+$ DCs, CLEC9A and XCR1 were quite low in our DC
614 populations, which has been previously described (24). The complex environment and array
615 of signals DC progenitors are exposed to during development presents a challenge to
616 replicate *in vitro*. However, fundamental understanding of human DC development is
617 expanding, and in the future knowledge of detailed changes in the transcriptional profile of
618 these cells during development can be applied to help refine differentiation protocols.
619 However, iPS-DCs described herein expressed multiple DC lineage markers, suggesting that
620 our differentiation protocol is sufficient to derive DC-like cells. In addition, we demonstrated
621 that after differentiation into iPSDMs, $IRF5^{-/-}$ cells are also deficient in IL-6 and TNF-α
622 production, demonstrating for the first time that virus induced immune responses, including

cytokine secretion, can be investigated in iPS-derived cells of multiple myeloid lineages that contain biallelic mutations, thus demonstrating the flexibility of iPSCs as tools to study immune responses to pathogens in multiple cell types.

In two independent studies response eQTLs (reQTLs) were found in IRF5 after stimulation of cells with virus or TLR ligands (57, 58), suggesting that variation within the IRF5 locus may be important in driving differences in expression. It would be interesting in future studies to see if SNPs which drive higher IRF5 expression in human macrophages and DCs also correlate with a heightened inflammatory response to viruses such as IAV, as our data suggest that such individuals may be preferentially susceptible to influenza pathogenesis and imply that targeting high IRF5 levels in these individuals could reduce inflammation without impacting virus control. As well as being a useful tool to knockout genes to assess cell-specific function as we have shown here, iPS-DCs could also be used as a tool to explore how common human genetic variants are associated with immune cell responses to various pathogens.

Acknowledgements

This work was supported by The Wellcome Trust. This work was funded by a Wellcome Trust Senior Research Fellowship to Ian Humphreys (207503/Z/17/Z); Medical Research Council, United Kingdom (MR/L018942/1 and MRC Human Immunology Unit Core); Chinese Academy of Medical Sciences (CAMS) Innovation Fund for Medical Sciences (CIFMS), China (grant number: 2018-I2M-2-002). The Wellcome Trust Sanger Institute was the source of the Kolf2 human induced pluripotent cell line which was generated under the Human Induced Pluripotent Stem Cell Initiative funded by a grant from the Wellcome Trust

647 and Medical Research Council, supported by the Wellcome Trust (WT098051) and the
648 NIHR/Wellcome Trust Clinical Research Facility, and Life Science Technologies
649 Corporation provided Cytotune for reprogramming. We thank the Wellcome Trust Sanger
650 Institute Gene editing pipeline for generation of IRF5$^{-/-}$ iPSCs and the Mass spectrometry
651 Facility at the Weatherall Institute of Molecular Medicine for help with CyTOF experiments.

652

653 J.L.F., I.H., M.C., S.D., M.M., L.C. performed experiments in mice. J.L.F, E.L., E.C., C.T.,
654 S.C., C.H. performed experiments using human iPSCs. A.Y. generated TALEN-engineered
655 IRF5$^{-/-}$ iPSCs. J.L.F. and D.W. performed experiments using human blood-derived DCs.
656 D.W. conducted CyTOF experiments and analyzed CyTOF data. I.U. provided *Irf5*$^{-/-}$ mice.
657 J.L.F, I.R.H, I.U., M.C., D.W. designed experiments. I.R.H., T.D. & G.D. supervised the
658 study. J.L.F. and I.R.H wrote the manuscript. All authors approved the final manuscript.

659

660 **References**

661 1. de Jong MD, Simmons CP, Thanh TT, Hien VM, Smith GJD, Chau TNB, Hoang DM,
662 Van Vinh Chau N, Khanh TH, Dong VC, Qui PT, Van Cam B, Ha DQ, Guan Y, Peiris
663 JSM, Chinh NT, Hien TT, Farrar J. 2006. Fatal outcome of human influenza A (H5N1)
664 is associated with high viral load and hypercytokinemia. Nat Med 12:1203–1207.
665 2. Humphreys IR, Walzl G, Edwards L, Rae A, Hill S, Hussell T. 2003. A Critical Role
666 for OX40 in T Cell–mediated Immunopathology during Lung Viral Infection. J Exp
667 Med 198:1237–1242.
668 3. GeurtsvanKessel CH, Willart MAM, van Rijt LS, Muskens F, Kool M, Baas C,
669 Thielemans K, Bennett C, Clausen BE, Hoogsteden HC, Osterhaus ADME,
670 Rimmelzwaan GF, Lambrecht BN. 2008. Clearance of influenza virus from the lung

671 depends on migratory langerin+CD11b− but not plasmacytoid dendritic cells. J Exp
672 Med 205:1621–1634.
673 4. Liu J, Cao X. 2016. Cellular and molecular regulation of innate inflammatory
674 responses. Cell Mol Immunol.
675 5. Iwasaki A, Pillai PS. 2014. Innate immunity to influenza virus infection. Nat Rev
676 Immunol 14:315–328.
677 6. Tavares LP, Teixeira MM, Garcia CC. 2017. The inflammatory response triggered by
678 Influenza virus: a two edged sword. Inflamm Res 66:283–302.
679 7. Khoyratty TE, Udalova IA. 2018. Diverse mechanisms of IRF5 action in inflammatory
680 responses. Int J Biochem Cell Biol 99:38–42.
681 8. Krausgruber T, Saliba D, Ryzhakov G, Lanfrancotti A, Blazek K, Udalova IA. 2010.
682 IRF5 is required for late-phase TNF secretion by human dendritic cells. Blood
683 115:4421–4430.
684 9. Douagi I, McInerney GM, Hidmark AS, Miriallis V, Johansen K, Svensson L,
685 Karlsson Hedestam GB. 2007. Role of Interferon Regulatory Factor 3 in Type I
686 Interferon Responses in Rotavirus-Infected Dendritic Cells and Fibroblasts. J Virol
687 81:2758–2768.
688 10. Honda K, Yanai H, Negishi H, Asagiri M, Sato M, Mizutani T, Shimada N, Ohba Y,
689 Takaoka A, Yoshida N, Taniguchi T. 2005. IRF-7 is the master regulator of type-I
690 interferon-dependent immune responses. Nature 434:772–777.
691 11. Ren J, Chen X, Chen ZJ. 2014. IKKβ is an IRF5 kinase that instigates inflammation.
692 Proc Natl Acad Sci 111:17438–17443.
693 12. Takaoka A, Yanai H, Kondo S, Duncan G, Negishi H, Mizutani T, Kano S, Honda K,
694 Ohba Y, Mak TW, Taniguchi T. 2005. Integral role of IRF-5 in the gene induction
695 programme activated by Toll-like receptors. Nature 434:243–249.

13. Eames HL, Corbin AL, Udalova IA. 2016. Interferon regulatory factor 5 in human autoimmunity and murine models of autoimmune disease. Transl Res 167:167–182.

14. Thackray LB, Shrestha B, Richner JM, Miner JJ, Pinto AK, Lazear HM, Gale M, Diamond MS. 2014. Interferon Regulatory Factor 5-Dependent Immune Responses in the Draining Lymph Node Protect against West Nile Virus Infection. J Virol 88:11007–11021.

15. Paun A, Bankoti R, Joshi T, Pitha PM, Stäger S. 2011. Critical Role of IRF-5 in the Development of T helper 1 responses to Leishmania donovani infection. PLoS Pathog 7:e1001246.

16. Yeung ATY, Hale C, Lee AH, Gill EE, Bushell W, Parry-Smith D, Goulding D, Pickard D, Roumeliotis T, Choudhary J, Thomson N, Skarnes WC, Dougan G, Hancock REW. 2017. Exploiting induced pluripotent stem cell-derived macrophages to unravel host factors influencing Chlamydia trachomatis pathogenesis. Nat Commun 8:15013.

17. Yanai H, Chen H -m., Inuzuka T, Kondo S, Mak TW, Takaoka A, Honda K, Taniguchi T. 2007. Role of IFN regulatory factor 5 transcription factor in antiviral immunity and tumor suppression. Proc Natl Acad Sci 104:3402–3407.

18. Mancl ME, Hu G, Sangster-Guity N, Olshalsky SL, Hoops K, Fitzgerald-Bocarsly P, Pitha PM, Pinder K, Barnes BJ. 2005. Two Discrete Promoters Regulate the Alternatively Spliced Human Interferon Regulatory Factor-5 Isoforms. J Biol Chem 280:21078–21090.

19. Lin KL, Suzuki Y, Nakano H, Ramsburg E, Gunn MD. 2008. CCR2 + Monocyte-Derived Dendritic Cells and Exudate Macrophages Produce Influenza-Induced Pulmonary Immune Pathology and Mortality. J Immunol 180:2562–2572.

20. Ellis GT, Davidson S, Crotta S, Branzk N, Papayannopoulos V, Wack A. 2015.

TRAIL + monocytes and monocyte-related cells cause lung damage and thereby increase susceptibility to influenza– S treptococcus pneumoniae coinfection. EMBO Rep 16:1203–1218.

21. Osugi Y, Vuckovic S, Hart DNJ. 2002. Myeloid blood CD11c+ dendritic cells and monocyte-derived dendritic cells differ in their ability to stimulate T lymphocytes. Blood 100:2858–2866.

22. Hale C, Yeung A, Goulding D, Pickard D, Alasoo K, Powrie F, Dougan G, Mukhopadhyay S. 2015. Induced Pluripotent Stem Cell Derived Macrophages as a Cellular System to Study Salmonella and Other Pathogens. PLoS One 10:e0124307.

23. Leha A, Moens N, Meleckyte R, Culley OJ, Gervasio MK, Kerz M, Reimer A, Cain SA, Streeter I, Folarin A, Stegle O, Kielty CM, Durbin R, Watt FM, Danovi D. 2016. A high-content platform to characterise human induced pluripotent stem cell lines. Methods 96:85–96.

24. Sachamitr P, Leishman AJ, Davies TJ, Fairchild PJ. 2018. Directed Differentiation of Human Induced Pluripotent Stem Cells into Dendritic Cells Displaying Tolerogenic Properties and Resembling the CD141+ Subset. Front Immunol 8.

25. Wilgenburg B van, Browne C, Vowles J, Cowley SA. 2013. Efficient, Long Term Production of Monocyte-Derived Macrophages from Human Pluripotent Stem Cells under Partly-Defined and Fully-Defined Conditions. PLoS One 8:e71098.

26. Hussell T, Pennycook A, Openshaw PJM. 2001. Inhibition of tumor necrosis factor reduces the severity of virus-specific lung immunopathology. Eur J Immunol 31:2566–2573.

27. Vlahos R, Stambas J, Bozinovski S, Broughton BRS, Drummond GR, Selemidis S. 2011. Inhibition of Nox2 Oxidase Activity Ameliorates Influenza A Virus-Induced Lung Inflammation. PLoS Pathog 7:e1001271.

28. Chen X, Zhou L, Peng N, Yu H, Li M, Cao Z, Lin Y, Wang X, Li Q, Wang J, She Y, Zhu C, Lu M, Zhu Y, Liu S. 2017. MicroRNA-302a suppresses influenza A virus–stimulated interferon regulatory factor-5 expression and cytokine storm induction. J Biol Chem 292:21291–21303.

29. Davidson S, Crotta S, McCabe TM, Wack A. 2014. Pathogenic potential of interferon αβ in acute influenza infection. Nat Commun 5:3864.

30. Xu L, Yoon H, Zhao MQ, Liu J, Ramana C V., Enelow RI. 2004. Cutting Edge: Pulmonary Immunopathology Mediated by Antigen-Specific Expression of TNF-α by Antiviral CD8 + T Cells. J Immunol 173:721–725.

31. Song M-S, Cho Y-H, Park S-J, Pascua PNQ, Baek YH, Kwon H-I, Lee O-J, Kong B-W, Kim H, Shin E-C, Kim C-J, Choi YK. 2013. Early Regulation of Viral Infection Reduces Inflammation and Rescues Mx-Positive Mice from Lethal Avian Influenza Infection. Am J Pathol 182:1308–1321.

32. Forbester JL, Lees EA, Goulding D, Forrest S, Yeung A, Speak A, Clare S, Coomber EL, Mukhopadhyay S, Kraiczy J, Schreiber F, Lawley TD, Hancock REW, Uhlig HH, Zilbauer M, Powrie F, Dougan G. 2018. Interleukin-22 promotes phagolysosomal fusion to induce protection against Salmonella enterica Typhimurium in human epithelial cells. Proc Natl Acad Sci 115:10118–10123.

33. Mukhopadhyay S, Heinz E, Porreca I, Alasoo K, Yeung A, Yang H-T, Schwerd T, Forbester JL, Hale C, Agu CA, Choi YH, Rodrigues J, Capitani M, Jostins-Dean L, Thomas DC, Travis S, Gaffney D, Skarnes WC, Thomson N, Uhlig HH, Dougan G, Powrie F. 2020. Loss of IL-10 signaling in macrophages limits bacterial killing driven by prostaglandin E2. J Exp Med 217.

34. Collin M, Bigley V. 2018. Human dendritic cell subsets: an update. Immunology 154:3–20.

771 35. Colletti NJ, Liu H, Gower AC, Alekseyev YO, Arendt CW, Shaw MH. 2016. TLR3
772 Signaling Promotes the Induction of Unique Human BDCA-3 Dendritic Cell
773 Populations. Front Immunol 7.
774 36. Breton G, Zheng S, Valieris R, Tojal da Silva I, Satija R, Nussenzweig MC. 2016.
775 Human dendritic cells (DCs) are derived from distinct circulating precursors that are
776 precommitted to become CD1c+ or CD141+ DCs. J Exp Med 213:2861–2870.
777 37. Lauder SN, Jones E, Smart K, Bloom A, Williams AS, Hindley JP, Ondondo B, Taylor
778 PR, Clement M, Fielding C, Godkin AJ, Jones SA, Gallimore AM. 2013. Interleukin-6
779 limits influenza-induced inflammation and protects against fatal lung pathology. Eur J
780 Immunol 43:2613–2625.
781 38. Dienz O, Rud JG, Eaton SM, Lanthier PA, Burg E, Drew A, Bunn J, Suratt BT,
782 Haynes L, Rincon M. 2012. Essential role of IL-6 in protection against H1N1
783 influenza virus by promoting neutrophil survival in the lung. Mucosal Immunol 5:258–
784 266.
785 39. Kaiser L, Fritz RS, Straus SE, Gubareva L, Hayden FG. 2001. Symptom pathogenesis
786 during acute influenza: Interleukin-6 and Other cytokine responses. J Med Virol
787 64:262–268.
788 40. Hayden FG, Fritz R, Lobo MC, Alvord W, Strober W, Straus SE. 1998. Local and
789 systemic cytokine responses during experimental human influenza A virus infection.
790 Relation to symptom formation and host defense. J Clin Invest 101:643–649.
791 41. Lopez-Pelaez M, Lamont DJ, Peggie M, Shpiro N, Gray NS, Cohen P. 2014. Protein
792 kinase IKKβ-catalyzed phosphorylation of IRF5 at Ser462 induces its dimerization and
793 nuclear translocation in myeloid cells. Proc Natl Acad Sci 111:17432–17437.
794 42. Davidson S, Crotta S, McCabe TM, Wack A. 2014. Pathogenic potential of interferon
795 αβ in acute influenza infection. Nat Commun 5:3864.

796 43. Pang IK, Pillai PS, Iwasaki A. 2013. Efficient influenza A virus replication in the
797 respiratory tract requires signals from TLR7 and RIG-I. Proc Natl Acad Sci
798 110:13910–13915.
799 44. Zhang Z, Yuan B, Lu N, Facchinetti V, Liu Y-J. 2011. DHX9 Pairs with IPS-1 To
800 Sense Double-Stranded RNA in Myeloid Dendritic Cells. J Immunol 187:4501–4508.
801 45. Kandasamy M, Suryawanshi A, Tundup S, Perez JT, Schmolke M, Manicassamy S,
802 Manicassamy B. 2016. RIG-I Signaling Is Critical for Efficient Polyfunctional T Cell
803 Responses during Influenza Virus Infection. PLOS Pathog 12:e1005754.
804 46. Schoenemeyer A, Barnes BJ, Mancl ME, Latz E, Goutagny N, Pitha PM, Fitzgerald
805 KA, Golenbock DT. 2005. The Interferon Regulatory Factor, IRF5, Is a Central
806 Mediator of Toll-like Receptor 7 Signaling. J Biol Chem 280:17005–17012.
807 47. Silvin A, Yu CI, Lahaye X, Imperatore F, Brault J-B, Cardinaud S, Becker C, Kwan
808 W-H, Conrad C, Maurin M, Goudot C, Marques-Ladeira S, Wang Y, Pascual V,
809 Anguiano E, Albrecht RA, Iannacone M, García-Sastre A, Goud B, Dalod M, Moris
810 A, Merad M, Palucka AK, Manel N. 2017. Constitutive resistance to viral infection in
811 human CD141 + dendritic cells. Sci Immunol 2:eaai8071.
812 48. Iwasaki A, Pillai PS. 2014. Innate immunity to influenza virus infection. Nat Rev
813 Immunol 14:315–328.
814 49. Lazear HM, Lancaster A, Wilkins C, Suthar MS, Huang A, Vick SC, Clepper L,
815 Thackray L, Brassil MM, Virgin HW, Nikolich-Zugich J, Moses A V., Gale M, Früh
816 K, Diamond MS. 2013. IRF-3, IRF-5, and IRF-7 Coordinately Regulate the Type I
817 IFN Response in Myeloid Dendritic Cells Downstream of MAVS Signaling. PLoS
818 Pathog 9:e1003118.
819 50. Purtha WE, Swiecki M, Colonna M, Diamond MS, Bhattacharya D. 2012.
820 Spontaneous mutation of the Dock2 gene in Irf5-/- mice complicates interpretation of

type I interferon production and antibody responses. Proc Natl Acad Sci 109:E898–E904.

51. Andrilenas KK, Ramlall V, Kurland J, Leung B, Harbaugh AG, Siggers T. 2018. DNA-binding landscape of IRF3, IRF5 and IRF7 dimers: implications for dimer-specific gene regulation. Nucleic Acids Res 46:2509–2520.

52. Barnes BJ, Kellum MJ, Field AE, Pitha PM. 2002. Multiple regulatory domains of IRF-5 control activation, cellular localization, and induction of chemokines that mediate recruitment of T lymphocytes. Mol Cell Biol 22:5721–40.

53. Hatesuer B, Hoang HTT, Riese P, Trittel S, Gerhauser I, Elbahesh H, Geffers R, Wilk E, Schughart K. 2017. Deletion of ***Irf3*** and ***Irf7*** Genes in Mice Results in Altered Interferon Pathway Activation and Granulocyte-Dominated Inflammatory Responses to Influenza A Infection. J Innate Immun 9:145–161.

54. Ciancanelli MJ, Huang SXL, Luthra P, Garner H, Itan Y, Volpi S, Lafaille FG, Trouillet C, Schmolke M, Albrecht RA, Israelsson E, Lim HK, Casadio M, Hermesh T, Lorenzo L, Leung LW, Pedergnana V, Boisson B, Okada S, Picard C, Ringuier B, Troussier F, Chaussabel D, Abel L, Pellier I, Notarangelo LD, Garcia-Sastre A, Basler CF, Geissmann F, Zhang S-Y, Snoeck H-W, Casanova J-L. 2015. Life-threatening influenza and impaired interferon amplification in human IRF7 deficiency. Science (80-) 348:448–453.

55. Mestas J, Hughes CCW. 2004. Of mice and not men: differences between mouse and human immunology. J Immunol 172:2731–8.

56. Hockemeyer D, Jaenisch R. 2016. Induced Pluripotent Stem Cells Meet Genome Editing. Cell Stem Cell 18:573–586.

57. Lee MN, Ye C, Villani A-C, Raj T, Li W, Eisenhaure TM, Imboywa SH, Chipendo PI, Ran FA, Slowikowski K, Ward LD, Raddassi K, McCabe C, Lee MH, Frohlich IY,

Hafler DA, Kellis M, Raychaudhuri S, Zhang F, Stranger BE, Benoist CO, De Jager PL, Regev A, Hacohen N. 2014. Common Genetic Variants Modulate Pathogen-Sensing Responses in Human Dendritic Cells. Science (80-) 343:1246980–1246980.

58. Çalışkan M, Baker SW, Gilad Y, Ober C. 2015. Host Genetic Variation Influences Gene Expression Response to Rhinovirus Infection. PLOS Genet 11:e1005111.

Figure legends

Figure 1. IRF5 alters cytokine responses to Influenza A virus in a murine infection model. WT and *Irf5*$^{-/-}$ mice were infected intranasally with 3 x 10^3 A/X-31 influenza (**A**) Inflammatory cytokine expression in BAL, was measured using multiplex assays 2, 4 and 7 days p.i. Data shown as mean ± SEM using 7 WT and 5 *Irf5*$^{-/-}$ mice (day 2) or five mice per genotype (day 4 and day 7) and represents two independent experiments. (**B**) IFN-α and IFN-β levels in BAL measured by ELISA in *Irf5*$^{-/-}$ and WT naïve and IAV infected mice 2 days p.i. Data shown as mean ± SEM of 3-6 mice per group at 2 days p.i.

Figure 2. IRF5 enhances Influenza A virus-induced inflammatory response in a murine infection model. (**A**) Weight loss of WT and *Irf5*$^{-/-}$ mice was assessed over time and comparable results were observed in 4 independent experiments, with 4-5 WT or *Irf5*$^{-/-}$ mice in each group per experiment. Data shown as mean ± SEM. (**B**) Replicating virus in lung was quantified by plaque assay. Data shown as mean ± SEM using 7 WT and 5 *Irf5*$^{-/-}$ mice for day 2, and 5 mice of each genotype for day 4. (**C**) Recruitment of specific myeloid cell populations (mDCs, monocyte-derived DCs; cDCs, conventional DCs; pDCs, plasmacytoid DCs; Inflam. mon, inflammatory monocytes) in WT and *Irf5*$^{-/-}$ mice was assessed by flow cytometry 2 days p.i. Populations were defined by the following markers: Alveolar macrophages - SiglecF$^+$ CD11b$^+$ CD64$^+$ Ly6C$^-$; mDCs - SiglecF$^-$ CD11b$^+$ MHC II$^+$ CD11c$^+$ CD64$^+$ Ly6C$^+$; Interstitial macrophages - SiglecF$^-$ CD11b$^+$ MHC II$^+$ CD11c$^-$ CD64$^+$ Ly6C$^+$; Inflammatory monocytes - Siglec F$^-$ CD11b$^+$ MHC II$^-$ Ly6C$^+$ CD64$^+$; cDCs; MHC II$^+$ CD11c$^+$ Ly6C$^-$; pDCs – B220$^+$ SiglecH$^+$ MHC II^{low} CD11c^{low}; Eosinophils – SiglecF$^+$ CD11c$^-$ CD11b$^+$ Ly6C$^-$. Data shown as mean ± SEM using 11 WT and 10 *Irf5*$^{-/-}$ mice from multiple replicates. (**D**) The total number of each individual myeloid cell population

(unstimulated, ex vivo) positive for IL-6 and TNF-α expression by was detected by flow cytometry, with data presented representing mean total cell number per 10^5 cells of each cell type ± SEM. Data represents two experiments.

Figure 3. IRF5 expression in human lung cells. IRF5 expression by multiple cellular subsets derived from human lung tissue from independent donors was analyzed by CyTOF. (**A**) UMAP based on down sampled, concatenated files from lung samples from four donors using phenotypic markers. Post UMAP analysis, populations (colored by cell type as identified by lung CyTOF) were defined via the following markers: $CD4^+$ T cells, $CD3^+$ $CD4^+$ $CD20^-$; $CD8^+$ T cells, $CD3^+$ $CD20^-$ $CD8^+$; B cells, $CD3^-$ $CD20^+$; NK cells, $CD3^-$ $CD20^-$ $CD56^+$; $CD14^+$ Monocytes, $CD16^-$ $CD11b^+$ $CD14^+$ $HLA\text{-}DR^+$; $CD16^+$ Monocytes, $CD14^-$ $CD11b^+$ $CD16^+$ $HLA\text{-}DR^+$; Macrophages, $CD11b^+$ $CD68^+$ $HLA\text{-}DR^+$; pDCs, $CD123^+$ $CD11b^+$ $HLA\text{-}DR^+$; $CD141^+$ cDCs, $CD11b^+$ $HLA\text{-}DR^+$ $CD1c^-$ $CD141^+$; $CD1c^+$ cDCs, $CD11b^+$ $HLA\text{-}DR^+$ $CD1c^+$ $CD141^-$; Eosinophils, $Siglec8^+$ CD123-; Basophils, $Siglec8^+$ $CD123^+$ (**B**) Median IRF5 expression in populations identified in (**A**) from lung samples taken from four independent donors, corrected for non-specific staining using unpermeabilized controls for each sample, error bars represent ± SEM. (**C**) Median IRF5 expression in myeloid vs lymphoid cell subsets, error bars represent ± SEM.

Figure 4. *IRF5*$^{-/-}$ iPSCs, IRF5^{Comp} iPSCs and Kolf2 iPSCs can be differentiated into iPS-DCs which lack or express IRF5. CRISPR/Cas9 was used to generate biallelic mutations in *IRF5* in the Kolf2 background. $IRF5^{Comp}$ iPSCs were generated using TALEN-mediated integration of *IRF5* into the $IRF5^{-/-}$ background. (**A**) Relative expression of *IRF5* in iPSCs and iPS-DCs, relative to *GAPDH*. Data shown as four technical replicates per assay, with assays repeated three times from independent iPS-DC batches. (**B**) Flow cytometry showing

IRF5 expression in iPS-DCs generated from IRF5$^{-/-}$, IRF5^{Comp} and Kolf2 iPSCs. (**C**) Immunostaining for IRF5 in A/X-31 influenza (IAV) infected Kolf2 and IRF5$^{-/-}$ iPS-DCs (DAPI, blue; IRF5, green). (**D**) IL-6 and TNF-α production 24h p.i. by A/X-31 influenza (IAV) challenged Kolf2 iPS-DCs and monocyte-derived DCs generated from human peripheral blood, either with or without 48h LPS maturation, was assayed by ELISA. Data represented shows mean ± SEM from three independent Kolf2 differentiations for iPS-DCs, and from three independent healthy donors for monocyte-derived DCs.

Figure 5. *IRF5*$^{-/-}$ iPSCs, IRF5^{Comp} iPSCs and Kolf2 iPSCs can be differentiated into iPS-DCs that display similar morphology. *IRF5*$^{-/-}$ iPSCs, IRF5^{Comp} and Kolf2 iPSCs were differentiated into dendritic cells using defined concentrations of growth factors to generate embryoid bodies (EBs), and GM-CSF and IL-4 to generate immature DCs from these EBs. (**A**) Total cell numbers of DC precursors harvested from DC differentiation plates. Data shown as 8 independent differentiations per iPSC line. (**B**) Surface expression of DC markers was examined via flow cytometry in Kolf2, IRF5$^{-/-}$ and IRF5^{Comp} iPS-DCs. Representative plots presented from one experiment, with experiments performed at least three times. (**C**) Gene expression of DC markers *CD83* and *CD86* and iPSC markers *NANOG* and *POU5F1* by iPS-DCs, relative to *GAPDH* was quantified using TaqMan gene-expression assays. Data shown represents four technical replicates per assay, with assays repeated at least twice from independent iPS-DC batches. (**D**) Morphology of iPS-DCs generated from Kolf2, IRF5^{Comp} and IRF5$^{-/-}$ iPSCs.

Figure 6. IRF5 enhances IAV-induced inflammatory cytokine production in iPS-DCs and iPSDMs. (**A**) IL-6 and TNF-α were measured by ELISA in supernatants harvested from iPS-DCs and iPSDMs generated from an iPSC line with a biallelic mutation in *IRF5*,

compared to the parent line Kolf2, and a line with a functional *IRF5* gene reintroduced into the AAVS1 integration site by TALEN engineering, after infection with IAV at MOI 1. Supernatants were harvested at 24 hours for assays; data shown represents mean ± SEM for triplicate wells from at least 3 independent experiments. (**B**) $IRF5^{-/-}$, $IRF5^{Comp}$ and Kolf2 iPS-DCs were infected with IAV at MOI 1, and then stained for IAV NP 24 hours post-infection and analyzed via flow cytometry (**C**) % positive NP iPS-DCs 24-hour IAV post-infection, with data presented showing mean ± SEM from three independent experiments. (**D**) Expression of DC maturation surface markers for iPS-DCs generated from $IRF5^{-/-}$, Kolf2 or $IRF5^{Comp}$ hIPSCs 24-hour post-infection with A/X-31 influenza (IAV), MOI 1, as measured by flow cytometry, with data presented showing mean ± SEM from three independent experiments.

Figure 7. Type I IFN signaling enhances IL-6 and TNF-α production by iPS-DCs. 2 x 10^4 iPS-DCs were challenged as stated below for each assay, and supernatants were harvested after 24 hours, unless otherwise stated. A/X-31 influenza (IAV) was used at MOI 1. (**A**) Cells were pre-incubated for 1-hour with anti-IFNAR1 antibody, or left untreated prior to viral infection. Data shown represents mean ± SEM for triplicate wells from at least 3 experiments. Supernatants were harvested and assayed for IL-6 and TNF-α by ELISA. (**B**) Supernatants from mock or IAV-infected Kolf2 or $IRF5^{-/-}$ iPS-DCs were harvested at 24 hours and assayed for IFN-α and IFN-β by ELISA. Data shown represents 2 separate experiments.

Figure 8. IRF5 acts downstream of TLR7 and RIG-I to drive inflammatory cytokine responses in iPS-DCs. 2 x 10^4 iPS-DCs were challenged as stated below for each condition in each assay and supernatants were harvested after 24 hours. A/X-31 influenza (IAV) was

used at MOI 1. For blocking assays cells were either pre-incubated for 1 hour with inhibitor (IMD 0354; IKKβ inhibitor) or inhibitor was added directly with viral inoculum (ODN 20958; TLR7 inhibitor). Data shown represents mean ± SEM for triplicate wells from at least 3 experiments, unless otherwise stated. (**A**) IL-6 production by Kolf2 and IRF5$^{-/-}$ iPS-DCs in response to stimulation with various TLR ligands (TLR2: Pam3CSK4, 300 ng/mL; TLR3: Poly I:C, 50 μg/mL; TLR4: LPS, 50 μg/mL; TLR7: Imiquimod, 50 μg/mL; TLR9: ODN 2216, 3 μg/mL) was measured by ELISA. Data shown represents four wells per condition for one iPS-DC batch per line, with assays replicated in two independent experiments. (**B**) IL-6 response as measured by ELISA in Kolf2 and IRF5$^{-/-}$ iPS-DCs to RIG-I ligand 3p-hpRNA with or without IKKβ inhibitor IMD 0354; and to A/X-31 influenza (IAV) with or without IMD 0354. (**C**) Fold-change in mRNA levels for *TLR7* and *DDX58*, measured by RT-qPCR using *GAPDH* as an endogenous control. (**D**) *DDX58* and *TLR7* mRNA levels in iPS-DCs after A/X-31 influenza (IAV) infection with or without blocking of type I IFN signaling using anti-IFNAR1. Data shown represents four technical replicates per assay, with assays repeated at least twice from independent iPS-DC batches. (**E**) Relative mRNA levels of *TLR7* in iPS-DCs generated from IRF5$^{-/-}$ iPSCs or parent Kolf2 iPSCs, measured using RT-qPCR. (**F**) IL-6 response as measured by ELISA in Kolf2 and IRF5$^{-/-}$ iPS-DCs to A/X-31 influenza with or without TLR7 inhibitor ODN 20958.

Figures

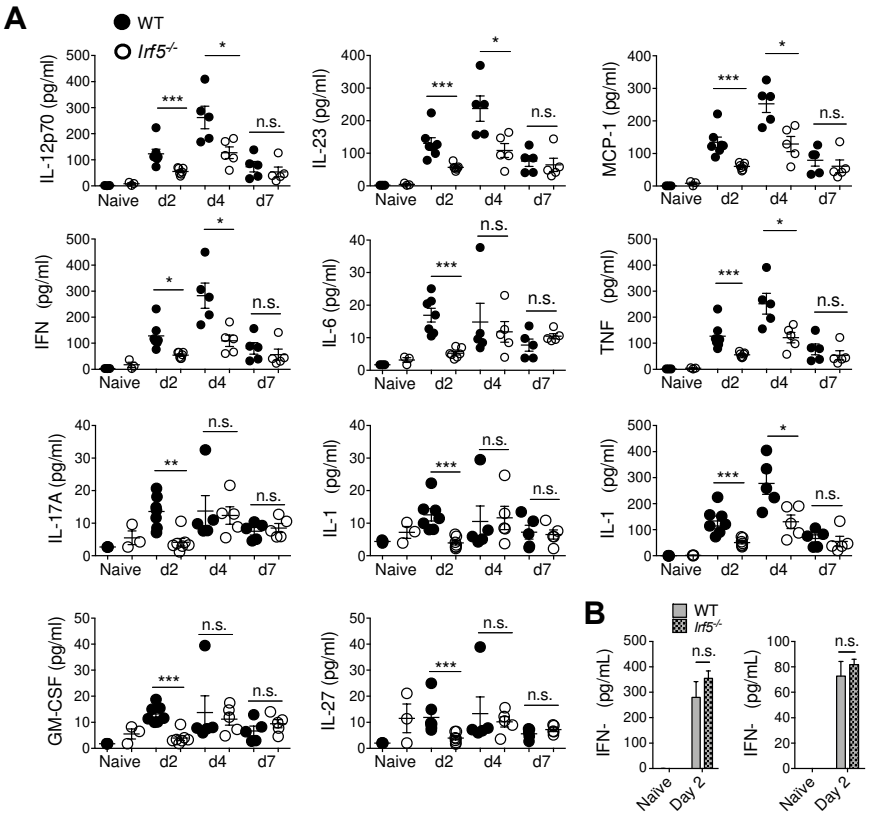

Figure 1.

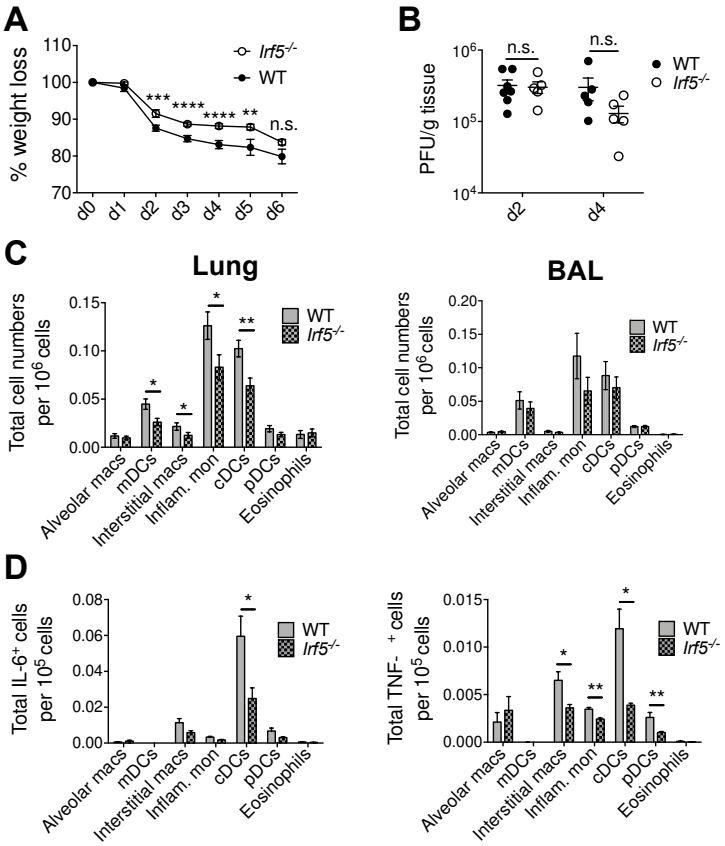

Figure 2.

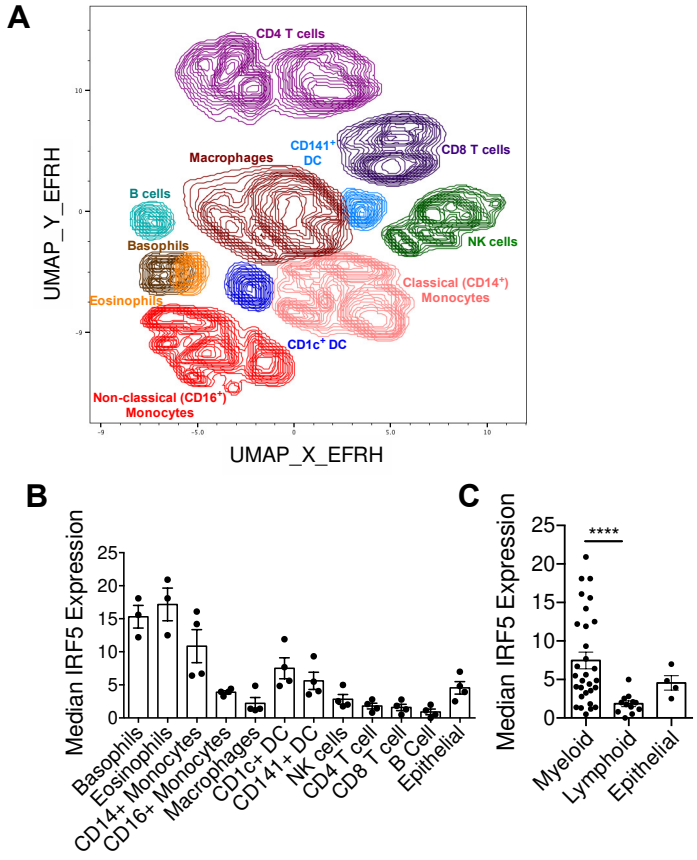

Figure 3.

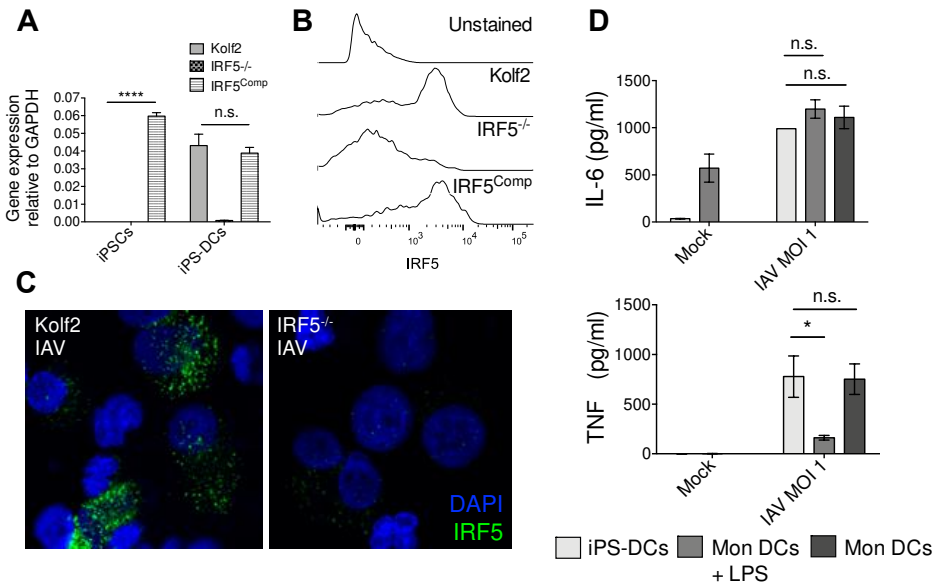

Figure 4.

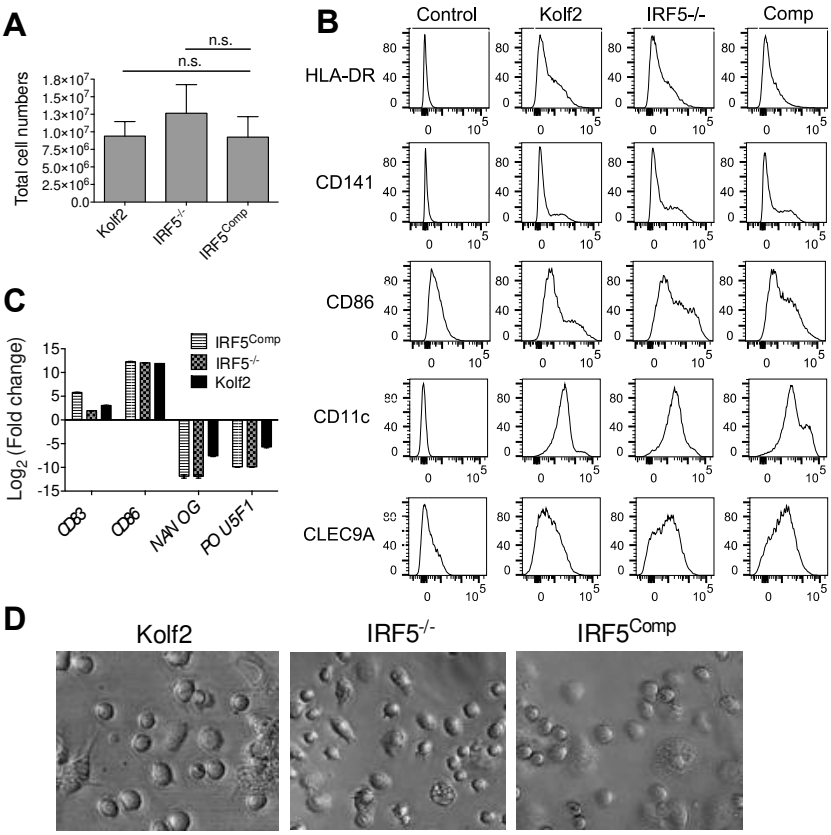

Figure 5.

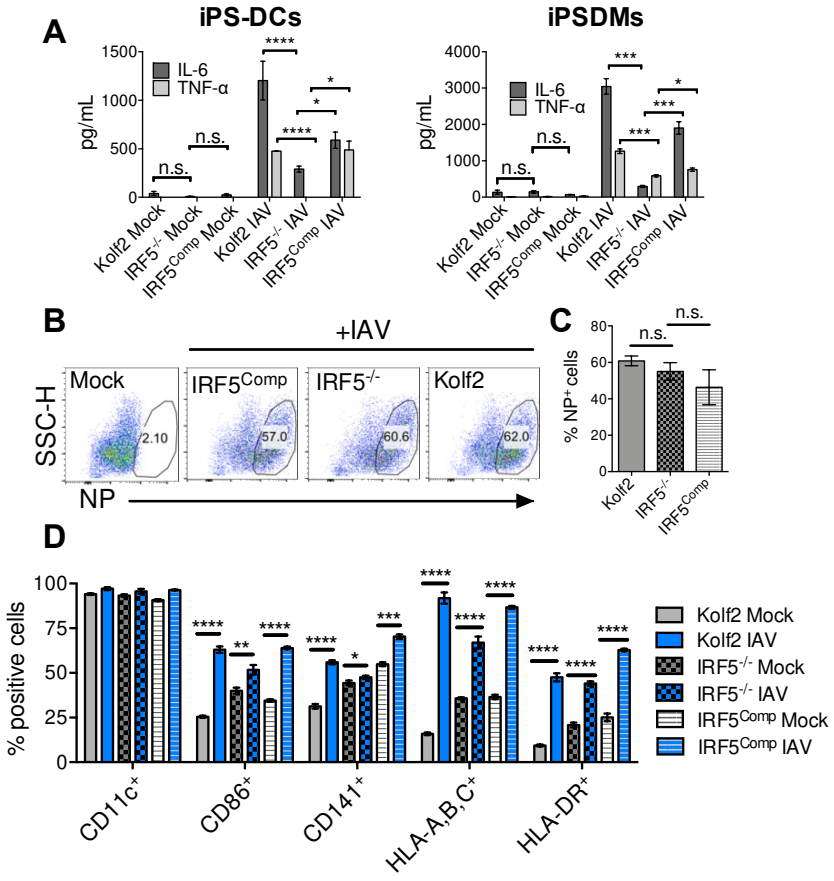

Figure 6.

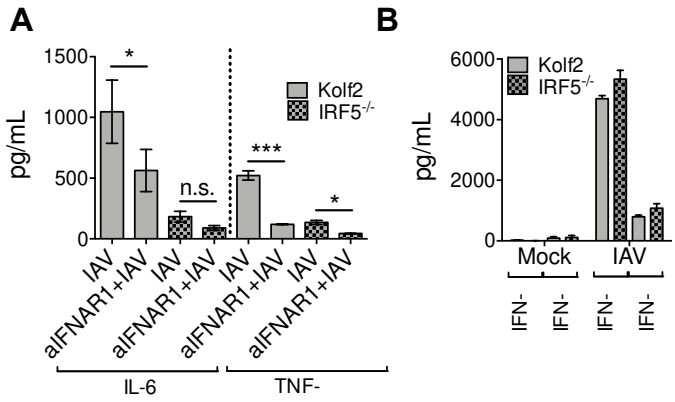

Figure 7.

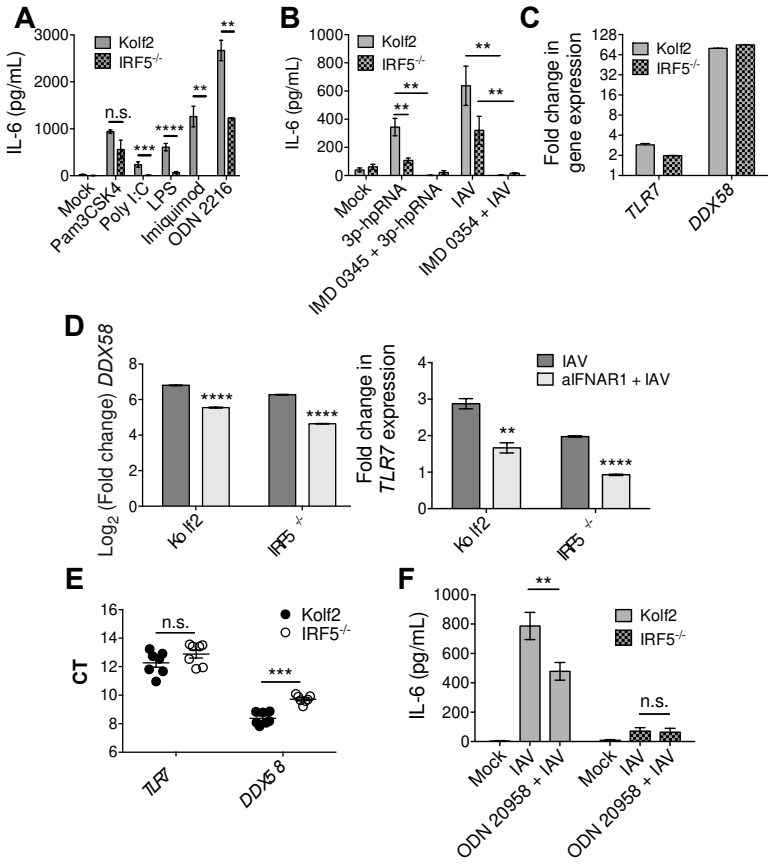

Figure 8.